PLANT IMMUNITY

Surface immune signaling unlocks NLR activation through mRNA alternative splicing

Chuyun Gao[1]†, Xi Meng[1]†, Xianchu Chen[1], Leiyun Yang[1], Tarhan Ibrahim[2], AmirAli Toghani[3], Enoch Lok Him Yuen[2], Nick Eilmann[2], Freddie King[2], Kangping Li[1], Luyao Wang[1], Biying Sun[1], Yuanchao Wang[1], Tolga Osman Bozkurt[2]*, Suomeng Dong[1]*

Plants activate pattern-triggered immunity (PTI) and effector-triggered immunity (ETI) to combat pathogens. However, how these systems coordinate immune activation while preventing autoimmunity remains poorly understood. In this study, we uncovered a regulatory mechanism in which surface immune signaling unlocks nucleotide-binding leucine-rich repeat (NLR) immune receptor activation through mRNA splicing. We identified an N-terminal prodomain in the potato late blight resistance protein Rpi-vnt1.1 that inhibits resistosome formation, preventing potential autoactivation of this NLR. Upon pathogen perception, PTI signaling induced alternative splicing of Rpi-vnt1.1 mRNA, removing this inhibitory element. This primed Rpi-vnt1.1 for activation by the *Phytophthora infestans* effector AVRvnt1, enabling resistosome assembly and immune signaling. The widespread conservation of N-terminal extensions in coiled coil–type NLRs points to a common regulatory mechanism in preventing potential autoactivation while preserving pathogen sensitivity.

Plants rely on cell surface and intracellular immune receptors to sense pathogens and execute immune responses that eliminate pathogens (*1*, *2*). Extracellular cues are recognized by cell surface–localized pattern recognition receptors (PRRs), which recognize conserved microbial features called pathogen-associated molecular patterns (PAMPs) (*3*–*8*). PRRs signal through coreceptors, such as SOBIR1 and BAK1, to elicit a range of basal defense responses (*9*). These responses include production of defense hormones, the burst of reactive oxygen species (ROS), and defense-related genes activation constituting PAMP-triggered immunity (PTI) (*10*). A separate class of immune receptors, nucleotide-binding domain leucine-rich repeat (NLR) proteins, detects host-translocated pathogen effectors intracellularly (*11*). In effector-triggered immunity (ETI), NLRs recognize these effectors and assemble resistosomes, oligomeric complexes that activate immune signaling and trigger hypersensitive response (HR) cell death to restrict infection (*12*). Although PTI and ETI were historically thought to work in isolation, growing evidence suggests they act in synergy. ETI enhances PTI by amplifying defense gene expression, whereas PTI modulates NLR activation through transcriptional and posttranslational mechanisms (*13*–*16*). Despite these advances, the precise mechanisms by which PTI regulates ETI activation remain poorly understood.

In most canonical coiled coil (CC)–type NLRs (CNLs), the α1 helix contains the MADA motif, which is essential for resistosome formation and immune activation (*17*–*19*). The MADA motif forms the tip of the funnel-shaped resistosome, which inserts into the plasma membrane to trigger the HR cell death response (*20*). Certain NLRs, including the agronomically important potato late blight resistance protein Rpi-vnt1.1, contain an N-terminal extension preceding the MADA motif, but its function remains unknown (*17*). In this study, we investigate the role of PTI in regulating NLR activation. The results reveal how surface immune signaling promotes Rpi-vnt1.1 activation through alternative splicing, providing new insights into the interplay between PTI and ETI.

PTI is required for the full activation of Rpi-vnt1.1-mediated immunity

To examine whether PTI enhances Rpi-vnt1.1–mediated immunity, we transiently expressed AVRvnt1 under a Dex-inducible promoter in *Rpi-vnt1.1*–transgenic *Nicotiana benthamiana* plants (Fig. 1A). The Rpi-vnt1.1–expressing leaves were treated with mock or three PAMPs (INF1, flg22, nlp20), respectively (*4*, *5*, *21*). We included nlp20 as a negative control, as *N. benthamiana* does not recognize it (*22*). Without Dex treatment, INF1 and flg22, but not nlp20, triggered ROS bursts and up-regulated the immune marker gene *NbACRE31* (fig. S1, A and B). Following Dex treatment, ion leakage increased substantially compared with that of untreated plants, indicating ETI activation through recognition of AVRvnt1 by Rpi-vnt1.1 (Fig. 1A). Subsequent treatment with INF1 or flg22 drastically accelerated Dex-induced ion leakage within 12 hours, whereas mock and nlp20 treatments did not (Fig. 1A). Similarly, INF1 and flg22 treatments enhanced Rpi-vnt1.1/AVRvnt1-induced hypersensitive response (HR) at 12 hours compared with mock and nlp20 treatments. At this timepoint, INF1 alone did not trigger HR, highlighting the synergistic effect of PTI activation (Fig. 1B). Additionally, 3,3′-diaminobenzidine (DAB) staining revealed that INF1 and flg22 treatments significantly increased H_2O_2 accumulation induced by Rpi-vnt1.1/AVRvnt1 (Fig. 1C). The observed modulation of Rpi-vnt1.1/AVRvnt1-mediated immunity by PTI could not be attributed to altered gene expression or protein accumulation, as neither Dex nor PAMP treatments largely influenced Rpi-vnt1.1 total mRNA or protein levels (figs. S1C and S2A). Similarly, PAMP treatment did not affect AVRvnt1 protein accumulation (fig. S2B).

We next investigated whether Rpi-vnt1.1–mediated immunity genetically requires PTI. We coexpressed Rpi-vnt1.1 and Dex:AVRvnt1 in previously characterized PTI-dependent coreceptor knock-out mutant plant *bak1* (*23*) as well as the TNL-dependent immune regulator mutant *eds1* (*24*), which served as a negative control. Following Dex treatment, Rpi-vnt1.1/AVRvnt1-induced ion leakage, HR, and H_2O_2 accumulation were notably reduced in *bak1* compared with those in the wild-type and *eds1* mutant (Fig. 1, D to F). The suppression of Rpi-vnt1.1/AVRvnt1-mediated immunity observed in *bak1* mutant was not attributable to differences in protein accumulation (fig. S2, C and D). Collectively, these data indicate that PRR signaling enhances Rpi-vnt1.1/AVRvnt1-mediated immunity and that the full activation of Rpi-vnt1.1–mediated immunity requires PRR signaling.

PTI promotes *Rpi-vnt1.1* mRNA splicing

We next investigated how PTI signaling regulates Rpi-vnt1.1 activity. We analyzed Rpi-vnt1.1 homologs across 47 potato genomes based on the observation of the N-terminal extension of Rpi-vnt1.1 (*25*). Results showed that the N-terminal extension is widely observed among Rpi-vnt1.1 family members (data S1). Notably, Rpi-vnt1.1 and its two alleles, Rpi-vnt1.2 and Rpi-vnt1.3, possess longer N-terminal extensions compared with most of Rpi-vnt1 homologs from other species. 5′ rapid amplification of complementary DNA ends (RACE) identified a U12-type intron (+138 to +237) in the 5′ region of *Rpi-vnt1.1* in the natural potato species *Solanum okadae* (Fig. 2A) (*26*–*28*). This splicing event produces two *Rpi-vnt1.1* transcript isoforms with distinct translation start sites: the N-terminally extended intron-retention (IR)

[1]State Key Laboratory of Agricultural and Forestry Biosecurity, Sanya Institute of Nanjing Agricultural University, The Key Laboratory of Integrated Management of Crop Diseases and Pests (Ministry of Education), College of Plant Protection, Nanjing Agricultural University, Nanjing, China. [2]Department of Life Sciences, Imperial College London, London, UK. [3]The Sainsbury Laboratory, University of East Anglia, Norwich Research Park, UK. ***Corresponding author. Email: smdong@njau.edu.cn (S.D.); o.bozkurt@imperial.ac.uk (T.O.B.)** †These authors contributed equally to this work.

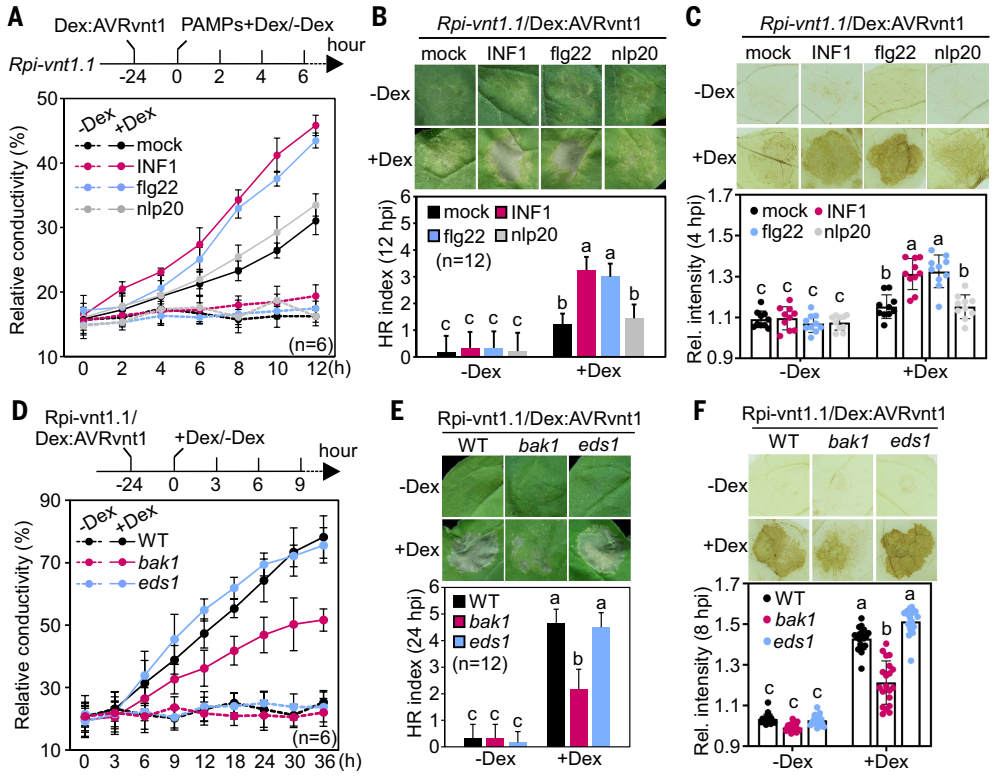

Fig. 1. Rpi-vnt1.1–mediated immunity requires *BAK1*. (**A** to **C**) The ion leakage (A), HR (B), and H_2O_2 accumulation (C) phenotype induced by Rpi-vnt1.1/AVRvnt1 upon PAMP treatments. *Rpi-vnt1.1*-transgenic *N. benthamiana* leaves were infiltrated with the *Agrobacteria* carrying Dex:AVRvnt1 24 hours before treatment with 10 μM dexamethasone (Dex) and buffer control (mock) or 0.5 μM INF1, 100 nM flg22, 100 nM nlp20, respectively. The HR phenotypes were photographed (up) and measured (down) 12 hours post-infiltration (hpi). The leaves stained by DAB were photographed (up) and measured (down) by ImageJ at 4 hpi. Relative staining intensity was compared to the untreated area. (**D** to **F**) The ion leakage (D), HR (E), and H_2O_2 accumulation (F) phenotype induced by Rpi-vnt1.1/AVRvnt1 in different *N. benthamiana* plants. Leaves of wild-type (WT), *bak1*, or *eds1* plants were infiltrated with *Agrobacteria* carrying Rpi-vnt1.1 and Dex:AVRvnt1-RFP 24 hours before treatment with 10 μM Dex. The HR phenotype was photographed (up) and measured (down) at 24 hpi. The leaves stained by DAB were photographed (up) and measured (down) by ImageJ at 8 hpi. Values and error bars represent means and SDs from three independent experiments, respectively. Different letters indicate statistically significant differences among groups as determined by one-way ANOVA followed by Tukey's multiple comparison test ($P < 0.05$).

isoform (*Rpi-vnt1.1*^{IR}) and the intron-spliced (IS) isoform (*Rpi-vnt1.1*^{IS}) with the N-terminal canonical MADA motif leader (Fig. 2A and fig. S3). To assess whether this feature is common among NLRs, we screened 4370 MADA-NLRs from 133 angiosperm genomes and found 218 of them have similar N-terminal extensions. Among these, 87 contain a second methionine at the beginning of their MADA motif (fig. S4A). Further analysis of 8530 MADA-NLRs from 346 reannotated *Solanaceae* genomes identified 619 with this feature (fig. S4B). These Solanaceae N-extended NLRs are phylogenetically closer to singleton NLRs, such as *Rpi-vnt1.1*, suggesting a potentially specific regulatory mechanism (fig. S5).

Because the retention of N terminus indicated possible masking of the MADA motif oligomerization and membrane insertion, we hypothesized that PTI promotes *Rpi-vnt1.1* alternative splicing (AS) to unmask the MADA motif. We first performed transcriptome sequencing of *S. okadae* treated with flg22 and found that the *Rpi-vnt1.1* gene exhibited alternative splicing at its 5′ end (Fig. 2B). We further validated this by monitoring the alternatively spliced isoforms of *Rpi-vnt1.1* in *S. okadae* plants upon PAMP treatment using reverse transcription polymerase chain reaction (RT-PCR). Notably, INF1 and flg22, but not nlp20 or mock treatment, promoted *Rpi-vnt1.1* mRNA splicing without largely affecting the total transcript levels of *Rpi-vnt1.1* and the reference gene *ELF1α* (Fig. 2C and fig. S6, A and D). Furthermore, similar results were obtained when examining *Rpi-vnt1.1* splicing in wild species *Solanum venturii*, advanced breeding line *Solanum tuberosum*^{C1848}, and the Desiree$^{Rpi\text{-}vnt1.1}$ transgenic line (Fig. 2D). Consistent with findings in the *Rpi-vnt1.1*–transgenic *N. benthamiana* (fig. S1), INF1 and flg22, but not nlp20 or mock treatment, triggered typical PTI responses in potatoes, including ROS bursts and activation of defense marker gene expression, validating their activities in potato (fig. S6, B, C, E, and F). However, we did not observe INF1-induced HR on the Desiree potato leaf, which is consistent with the previous report (*3*).

To determine whether this regulation occurs more broadly at the transcriptome level, we analyzed RNA sequencing (RNA-seq) data from *S. lycopersicum* cv. Moneymaker treated with PehC (*29*), the previous *S. okadae* dataset (Fig. 2B), and *Arabidopsis* Col-0 treated with flg22 (*30*). We identified PTI-induced U2-type differential alternative splicing (DAS) events in NLR genes and U12-type DAS event in surface receptor gene from the datasets (fig. S7). These were validated by RT-PCR, confirming that widespread alternative splicing of immune receptor genes occurs during PTI (fig. S7).

To assess the impact of PAMP treatment on Rpi-vnt1.1 variant abundance at the protein level, we performed parallel reaction monitoring (PRM) mass spectrometry. We designed an isoform-resolved peptide strategy using two reporters: a peptide specific to Rpi-vnt1.1^{IR}, and a peptide shared by both Rpi-vnt1.1^{IR} and Rpi-vnt1.1^{IS} to quantify total Rpi-vnt1.1 protein in *S. okadae* (Fig. 2E and fig. S8A). Both peptides were robustly detected in untreated samples; however, flg22 treatment markedly reduced the Rpi-vnt1.1^{IR}–specific signal (Fig. 2F and fig. S8B). Quantification of the IR/total ratio confirmed that flg22 significantly decreased the relative proportion of Rpi-vnt1.1^{IR} (Fig. 2G). These data demonstrate that PTI activation shifts Rpi-vnt1.1 isoform balance toward the immune signaling–competent Rpi-vnt1.1^{IS} variant at the protein level. We further developed a YFP splicing reporter (YSR) by fusing the *Rpi-vnt1.1* N-terminal sequence (+1 to +312 bp)—including the untranslated region (UTR), intron, and MADA motif coding sequence—to YFP. We also generated control constructs: YSR^{IR}, which contains the intron and MADA sequence, and YSR^{IS}, which includes only the MADA sequence, starting from the second TSS (Fig. 2H). When transiently expressed in *N. benthamiana*, YSR predominantly produced the YSR^{IR} protein variant (35 kDa), which was more abundant than the YSR^{IS} variant (31 kDa) (Fig. 2I). Upon INF1 or flg22 treatment, however, the abundance of YSR^{IS} increased, surpassing that of YSR^{IR} (Fig. 2J). Together, these results demonstrate that PTI signaling promotes alternative splicing of *Rpi-vnt1.1*, ensuring production of a resistosome-competent isoform (Rpi-vnt1.1^{IS}) in response to pathogen detection.

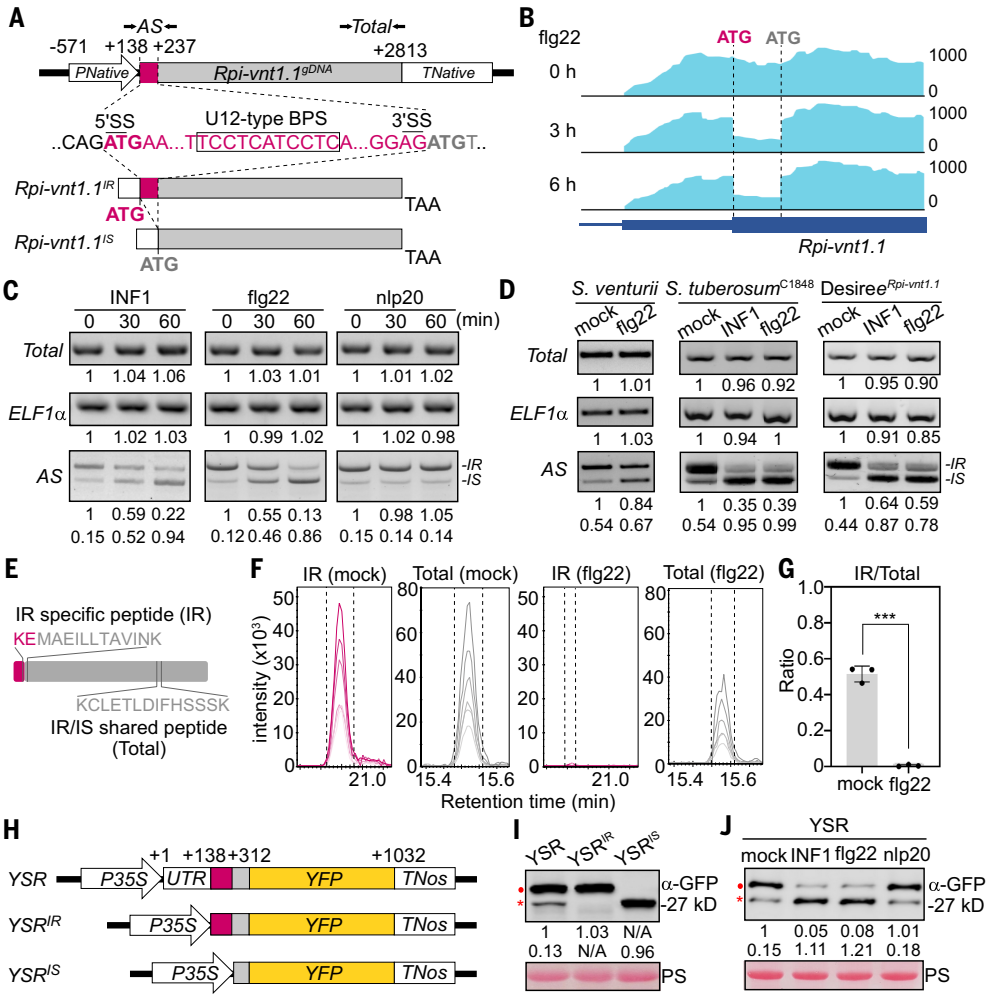

Fig. 2. PTI promotes *Rpi-vnt1.1* mRNA splicing. (**A** and **B**) RNA sequencing of *Rpi-vnt1.1* in *S. okadae* upon flg22 treatment. Schematic diagram of *Rpi-vnt1.1* open reading frame in *S. okadae* is shown in (A). Two *Rpi-vnt1.1* isoforms *Rpi-vnt1.1*^{IR} and *Rpi-vnt1.1*^{IS} were detected by 5′ RACE assay. The translation start sites (ATG) of two transcripts are bolded. The predicted U12-type intron (red), 5′ splice site (SS), U12-type branch point site (BPS), and 3′ SS are shown. Genomic visualization showing the read coverage from RNA-seq across the 5′ coding region of *Rpi-vnt1.1* locus (B). (**C** and **D**) RT-PCR analysis of *Rpi-vnt1.1*–containing potatoes. Primers for detecting total mRNA (*Total*) and the alternative splicing region (*AS*) are indicated by black bars in (A). *ELF1α* was used as reference gene. Numbers indicate relative abundance of different bands compared with the reference quantified by ImageJ (set as 1). The representative bands of *Rpi-vnt1.1*^{IR} and *Rpi-vnt1.1*^{IS} are indicated as *IR* and *IS*, respectively. (**E**) Peptide strategy for PRM quantification of Rpi-vnt1.1 protein in *S. okadae*. An IR-specific peptide was used to selectively monitor the Rpi-vnt1.1^{IR} variant, whereas a peptide shared between IR and IS variants was used to represent total Rpi-vnt1.1 protein abundance. (**F**) Representative extracted ion chromatograms from PRM transitions corresponding to the IR-specific peptide and the shared total peptide in mock- and flg22-treated *S. okadae* leaves. Different traces correspond to different fragment ions. Peak boundaries used for quantification are indicated. (**G**) Quantification of the IR/total peptide ratio following flg22 treatment. Bars represent mean ± SD from biological replicates. Asterisks indicate statistical significance (Student's *t* test; ***$P < 0.001$). (**H**) The schematic illustration of three constructs with YFP fusing the N terminal of Rpi-vnt1.1 genomic DNA sequences (*YSR*) and its two isoforms (*YSR*^{IR} and *YSR*^{IS}). (**I**) Western blot detection of YSR, YSR^{IR}, or YSR^{IS} expressed in *N. benthamiana*. (**J**) Western blot detection of YSR expressed in *N. benthamiana* after treatment with mock or PAMPs. In (I) and (J), the predicted YSR^{IR} and YSR^{IS} variants are indicated by a red dot and a red asterisk, respectively. Numbers indicate relative abundance of different bands compared with the reference quantified by ImageJ (set as 1). Protein loading is indicated by PS.

Alternative splicing generates a functional N-terminally truncated Rpi-vnt1.1 isoform that activates immunity

N-terminal tagging of canonical singleton or helper-type CC-NLRs typically impairs the HR response. Based on this, we reasoned that PTI primes *Rpi-vnt1.1* by promoting the accumulation of the spliced *Rpi-vnt1.1*^{IS} isoform, which encodes a classical MADA-NLR lacking the N-terminal extension that otherwise suppresses the HR. To test this, we evaluated the function of using engineered mutations in the YSR system to selectively express each isoform. To preserve intron retention, we mutated multiple U12 splicing acceptor sites (YSR^{IR1}) or replaced the second methionine (start codon) with alanine (YSR^{IR2}). To enforce intron splicing, we truncated the intron upstream of the MADA motif (YSR^{IS1}) or mutated the first methionine to alanine (YSR^{IS2}) (Fig. 3A). Western blot analysis confirmed that each construct produced protein bands of expected sizes, except YSR^{IR1}, which also produced a faint, slightly smaller band, likely a subtly spliced variant (Fig. 3B). Furthermore, PAMP treatment did not alter isoform expression, indicating that these mutations render YSR constructs insensitive to PTI-regulated splicing (Fig. 3B).

Having validated the functionality of YSR mutations, we next introduced them into full-length *Rpi-vnt1.1* to generate *Rpi-vnt1.1*^{IR1}, *Rpi-vnt1.1*^{IR2}, *Rpi-vnt1.1*^{IS1}, and *Rpi-vnt1.1*^{IS2} constructs. As a control, we generated an inactive mutant, *Rpi-vnt1.1*^{KN}, by substituting the lysine at residue 224 in the P-loop motif with asparagine, a broadly conserved inactivating mutation in NLRs (fig. S9A). Coexpression with Dex:AVRvnt1 revealed that *Rpi-vnt1.1*^{IS1} and *Rpi-vnt1.1*^{IS2} triggered substantially faster and stronger immune responses than wild-type *Rpi-vnt1.1*, including increased ion leakage, HR cell death, and H_2O_2 accumulation (Fig. 3, C to E). *Rpi-vnt1.1*^{IR1} elicited a weak immune response, consistent with inefficient splicing observed in the YSR system. *Rpi-vnt1.1*^{IR2}, on the other hand, failed to activate immunity, phenocopying the inactive P-loop mutant *Rpi-vnt1.1*^{KN}. All variants accumulated at levels comparable to wild-type *Rpi-vnt1.1* (fig. S9B). Interestingly, the immune responses triggered by two Rpi-vnt1.1 variants were no longer enhanced by PTI, suggesting that PTI acts upstream of *Rpi-vnt1.1* at the level of mRNA splicing (fig. S10). To determine whether N-terminal extensions generally exert an inhibitory effect, we fused N-terminal extensions of varying lengths from the *Rpi-vnt1* family, as well as MADA-NLRs of other plant species, to the N terminus of Rpi-vnt1.1^{IS1}. HR assays revealed that N-terminal extensions shorter than 16 amino acids had little to no inhibitory effect on HR, whereas extensions longer than 16 amino acids markedly suppressed HR (fig. S11), proving that variable N-extensions exert similar inhibitory effect on Rpi-vnt1.1 function.

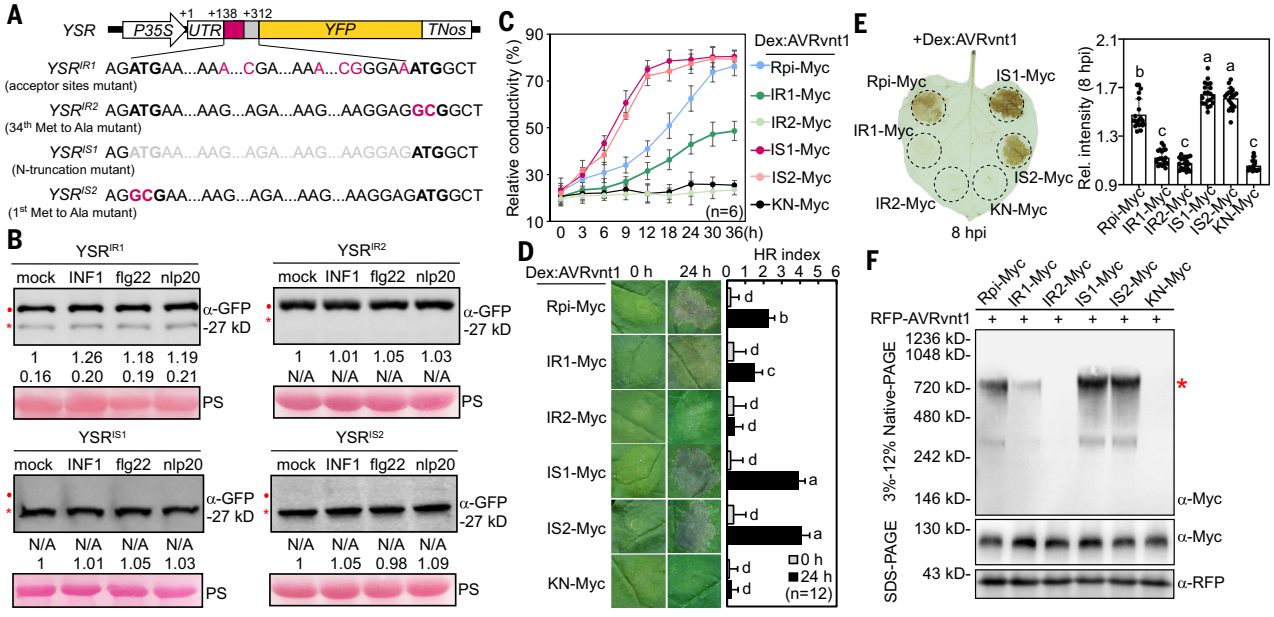

Fig. 3. mRNA splicing of *Rpi-vnt1.1* is required for its immune activation. (**A**) The schematic illustration of four YSR constructs with mutations on the N terminus. (**B**) Western blot detection of YSR mutants expressed in *N. benthamiana* after treatment with mock, 0.5 μM INF1, 100 nM flg22, or 100 nM nlp20, respectively. The total protein was extracted 3 hours after treatment for Western blot. The predicted YSR^{IR} and YSR^{IS} variants are indicated by a red dot and a red asterisk, respectively. Numbers indicate relative abundance of different bands compared with that of the reference quantified by ImageJ (set as 1). Protein loading was indicated by PS. (**C** to **E**) The ion leakage (C), HR (D), and H_2O_2 accumulation (E) phenotype induced by Rpi-vnt1.1–Myc (Rpi-Myc), Rpi-vnt1.1^{IR1}–Myc (IR1-Myc), Rpi-vnt1.1^{IR2}–Myc (IR2-Myc), Rpi-vnt1.1^{IS1}–Myc (IS1-Myc), Rpi-vnt1.1^{IS2}–Myc (IS2-Myc), or Rpi-vnt1.1^{KN}–Myc (KN-Myc). *N. benthamiana* leaves were infiltrated with *Agrobacteria* carrying indicated constructs 24 hours before treatment with 10 μM Dex. The HR phenotype was photographed (left) and measured (right) at 0 and 24 hpi. The leaves stained by DAB were photographed (left) and measured (right) by ImageJ at 8 hpi. Relative staining intensity was compared with that of the uninfiltrated area. Values and error bars represent means and SDs from three independent experiments, respectively. Different letters indicate statistically significant differences among groups as determined by one-way ANOVA followed by Tukey's multiple comparison test ($P < 0.01$). (**F**) The oligomerization of Rpi-Myc, IR1-Myc, IR2-Myc, IS1-Myc, IS2-Myc, or KN-Myc in the presence of AVRvnt1. The total protein of *N. benthamiana* expressing indicated constructs was extracted for BN-PAGE. The red asterisk indicates the oligomerized Rpi-vnt1.1.

Because CC-NLRs are known to form resistosomes during activation (*18*, *19*, *31*), we next tested whether Rpi-vnt1.1 oligomerizes upon activation. By using blue native polyacrylamide gel electrophoresis (BN-PAGE), we showed that wild-type Rpi-vnt1.1, as well as the spliced isoforms Rpi-vnt1.1^{IS1} and Rpi-vnt1.1^{IS2}, showed strong oligomerization upon activation by AVRvnt1. By contrast, Rpi-vnt1.1^{IR1} displayed markedly reduced oligomerization, whereas Rpi-vnt1.1^{IR2} and Rpi-vnt1.1^{KN} failed to oligomerize (Fig. 3F). Consistent with these results, we performed in vivo coimmunoprecipitation assays and found that Rpi-vnt1.1^{IS2} exhibited homoassociation only upon AVRvnt1 activation, whereas no interaction was detected between Rpi-vnt1.1^{IS2} and either Rpi-vnt1.1^{IR2} or the unrelated NLR RB under any condition (fig. S12). We further monitored Rpi-vnt1.1–induced Ca^{2+} influx using cell-based assays (*32*). The results showed that coexpression of Rpi-vnt1.1^{IR1} with AVRvnt1 triggered a weakened Ca^{2+} influx compared with wild-type Rpi-vnt1.1, whereas Rpi-vnt1.1^{IR2} completely lost its activity (fig. S13). To investigate the structural basis of this functional difference, we used AlphaFold3 Multimer to predict the resistosome structure of Rpi-vnt1.1 with and without the N-terminal extension. Our results showed that Rpi-vnt1.1^{IS} forms a stable resistosome with a well-ordered funnel-shaped architecture (fig. S14), whereas Rpi-vnt1.1^{IR} failed to assemble such a structure. We further curated 85 N-extended MADA-NLRs from diverse plants with different lengths of N-extension (data S9). In full-length isoforms, the N-terminal residues were consistently predicted as low-confidence, flexible segments (low pLDDT) that did not stabilize within the pore forming region and showed misplaced lipid engagements. Across species and N-extension lengths, these full-length models frequently displayed displacement or occlusion of the MADA α1 pore helix (fig. S14). These models support our experimental findings: Only the spliced isoform assembles into functional resistosomes capable of initiating defense. Together, these findings demonstrate that intron splicing of *Rpi-vnt1.1* is essential for its full activation to trigger immune responses, suggesting an autoinhibitory role of the N-terminal extension.

Rpi-vnt1.1 mRNA splicing is required for Rpi-vnt1.1–mediated late blight resistance

To evaluate the relevance of our findings during natural infection, we generated stable transgenic Desiree potato lines expressing either the IR (*Rpi-vnt1.1*^{IR1}) or IS isoform (*Rpi-vnt1.1*^{IS1}) under the control of the native *Rpi-vnt1.1* promoter. All *Rpi-vnt1.1*^{IS1} lines exhibited low expression levels and displayed quantitative resistance to *P. infestans* (Fig. 4A and B). This may reflect counterselection due to autoimmunity, as overexpression of untagged *Rpi-vnt1.1*^{IS1} in *N. benthamiana* induced a strong HR even without AVRvnt1 (Fig. 4C). By contrast, two independent *Rpi-vnt1.1*^{IR1} lines (#6 and #9) showed expression levels comparable with those of *Rpi-vnt1.1*-transgenic controls (fig. S15A). Consistent with our earlier observations (Fig. 3B), PAMP-induced mRNA splicing was strongly reduced in the *Rpi-vnt1.1*^{IR1} lines (fig. S15B). In both *S. okadae* and Desiree$^{Rpi\text{-}vnt1.1}$ potatoes inoculated with *P. infestans* strains T30-4, JH19, and P13527 (all expressing *AVRvnt1*) as well as the *AVRvnt1*-silenced strain P13626 (*33*), we observed enhanced *Rpi-vnt1.1* mRNA splicing without changes in total transcript levels, regardless of AVRvnt1 expression (Fig. 4D and fig. S16). Conversely, *Rpi-vnt1.1*^{IR1} mRNA splicing was only modestly induced under the same conditions (Fig. 4E).

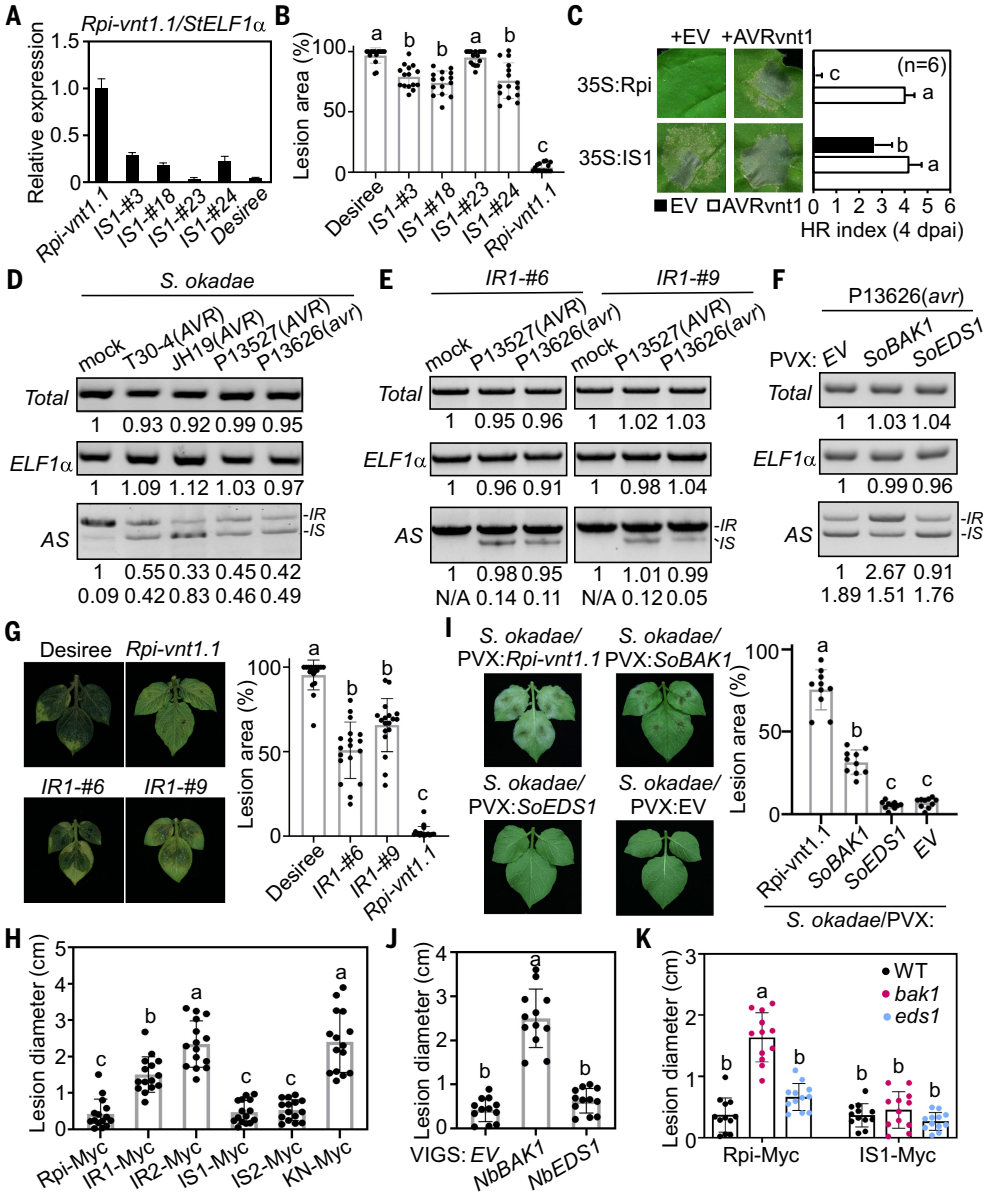

Fig. 4. PTI-induced mRNA splicing is required for Rpi-vnt1.1–mediated late blight resistance.
(**A**) RT-qPCR analysis of *Rpi-vnt1.1* in *Rpi-vnt1.1*^{IS1}-transgenic potatoes. (**B**) The lesion area measurement of *P. infestans* JH19 on Desiree$^{Rpi\text{-}vnt1.1}$ (*Rpi-vnt1.1*) and *IS1*. (**C**) The HR phenotype induced by 35S:Rpi-vnt1.1 and 35S:Rpi-vnt1.1^{IS1} with and without AVRvnt1 in *N. benthamiana*. The HR phenotype was photographed (left) and measured (right) at 4 dpai. (**D** to **F**) RT-PCR analysis of *Rpi-vnt1.1* in *S. okadae* upon *P. infestans* inoculation. Leaves of *S. okadae* were inoculated with deionized water (mock) or zoospore suspension of *P. infestans* T30-4, JH19, P13527, and P13626 in (D). Leaves of two independent lines of *Rpi-vnt1.1*^{IR1}–transgenic potato (*IR1*-#6 and *IR1*-#9) were inoculated with mock or zoospore suspension of *P. infestans* P13527 and P13626 in (E). Leaves of *S. okadae* potatoes after *PVX*-induced gene silencing were inoculated with mock or zoospore suspension of P13626 in (F). *AVR* and *avr* represent strains containing gene-expressed or -silenced *AVRvnt1*, respectively. Numbers indicated relative abundance of different bands compared with the reference quantified by ImageJ (set as 1). (**G** and **I**) The inoculation phenotype of *P. infestans* JH19 on Desiree$^{Rpi\text{-}vnt1.1}$ (*Rpi-vnt1.1*) and *IR1* (G) and *S. okadae* after *PVX*-induced gene silencing (*Rpi-vnt1.1*, *SoBAK1*, *SoEDS1*, *EV*) (I). (**H**, **J**, and **K**) The inoculation phenotype of *P. infestans* JH19 on *N. benthamiana* expressing Rpi-vnt1.1 and its mutants (H), *Rpi-vnt1.1*–transgenic *N. benthamiana* with gene silenced by VIGS (J), gene–knock-out *N. benthamiana* expressing Rpi-vnt1.1–Myc (Rpi-Myc) and Rpi-vnt1.1^{IS1}–Myc (IS1-Myc) (K). The lesion was measured by ImageJ at 4 dpai. Values and error bars represent means and SDs from three independent experiments, respectively. Different letters indicate statistically significant differences among groups as determined by one-way ANOVA followed by Tukey's multiple comparison test ($P < 0.01$).

To determine whether *P. infestans*–induced *Rpi-vnt1.1* mRNA splicing was due to PTI activation, we silenced *BAK1* in *S. okadae* using Potato virus X (PVX)–induced gene silencing (*34*), with *EDS1* silencing as a control (*35*). PVX mediated silencing of these genes substantially reduced their transcript levels, as expected, without affecting *Rpi-vnt1.1* expression (fig. S17). Notably, *BAK1* silencing greatly suppressed *P. infestans*–induced *Rpi-vnt1.1* mRNA splicing (Fig. 4F). We observed similar results in *N. benthamiana bak1* mutants (fig. S18), further confirming that *P. infestans*–induced *Rpi-vnt1.1* mRNA splicing requires PTI.

To assess the functional consequence, we examined late blight resistance in Desiree plants expressing Rpi-vnt1.1 or its variants. Ectopic expression of *Rpi-vnt1.1* conferred full resistance to *P. infestans*, whereas *Rpi-vnt1.1*^{IR1} lines displayed significantly reduced pathogen resistance (Fig. 4G). Similarly, in *N. benthamiana*, Rpi-vnt1.1^{IR1} and Rpi-vnt1.1^{IR2} mutants conferred weaker resistance compared with that of wild-type Rpi-vnt1.1, Rpi-vnt1.1^{IS1}, and Rpi-vnt1.1^{IS2} (Fig. 4H). We then asked whether the Rpi-vnt1.1–mediated disease resistance was dependent on PTI. Silencing *Rpi-vnt1.1* in *S. okadae* severely compromised late blight resistance, whereas silencing *BAK1* also reduced resistance but to a lesser extent (Fig. 4I). By contrast, silencing *EDS1* or *EV* control had no significant impact. A similar phenotype was observed in the Desiree$^{Rpi\text{-}vnt1.1}$ transgenic potato (fig. S19). Similarly, *NbBAK1* silencing in *Rpi-vnt1.1*–transgenic *N. benthamiana* also reduced resistance (Fig. 4J). To test whether PTI acts upstream of splicing, we transiently expressed Rpi-vnt1.1 or Rpi-vnt1.1^{IS} in the *N. benthamiana bak1* mutant. Rpi-vnt1.1–mediated resistance was diminished in the *bak1* mutant, but Rpi-vnt1.1^{IS1}–mediated resistance remained intact (Fig. 4K). These results demonstrate that PTI enhances Rpi-vnt1.1–mediated immunity by promoting alternative mRNA splicing. This mechanism acts as a regulatory checkpoint, suppressing potential NLR autoactivation while enabling rapid resistosome formation upon pathogen detection, thereby linking surface immune signaling to intracellular NLR activation.

Discussion

Accumulating evidence supports functional synergy between PTI and ETI, whereas the molecular mechanisms by which PTI regulates ETI remain poorly understood. Previous research showed that PTI can transcriptionally up-regulate certain *NLRs* (*30*). In this study, we identified a previously uncharacterized mechanism in which PTI enhances ETI by

promoting the alternative splicing of *Rpi-vnt1.1*, an agronomically important NLR conferring resistance to potato late blight. We show that the PTI signaling facilitates the removal of an inhibitory N-terminal extension from Rpi-vnt1.1 through mRNA splicing. The artificially spliced *Rpi-vnt1.1* isoforms (Rpi-vnt1.1^{IS}) are constitutively active and no longer responsive to PTI, suggesting that PTI acts upstream by enabling the production of Rpi-vnt1.1 into a functional, resistosome-competent receptor. Our findings unravel a mechanism in which PTI potentiates ETI through alternative splicing of an *NLR*, demonstrating how cells translate cell surface danger signals to prime their intracellular defenses while avoiding potential immune autoactivation in the absence of pathogen threat.

Our motif searching and structure modeling data suggest that the Rpi-vnt1.1 inhibitory modules may represent a broadly conserved strategy for negative regulation of NLRs. In resting conditions, this mechanism could suppress the potential autoactivation while allowing NLR transcript accumulation. Upon pathogen challenge, PTI could rapidly activate splicing to generate functional receptors, providing both robustness and restraint in immune deployment. Recent studies have further demonstrated that artificially fusing a cleavable peptide to the N terminus of NLRs enables controllable activation of these immune receptors (*36*), highlighting the broad application potential of the natural regulatory mechanism in this study.

Pathogen infection is known to induce widespread alternative splicing in plants (*37*). A notable parallel exists in mammals, where alternative splicing of *Gasdermin B* determines its pore-forming and pyroptotic activity upon caspase activation cascade (*38*). This highlights a common role for mRNA splicing in the functional modulation of immune-related proteins across kingdoms. But how does surface immune perception drive specific NLR splicing? Previous studies demonstrated that PAMP perception modulates alternative splicing of immune genes through phosphorylation cascades (*39*, *40*). Consistent with this, we observed that diverse PAMPs triggered Rpi-vnt1.1 splicing in both *N. benthamiana* and potato (Fig. 2). These findings suggest that PTI may recruit conserved pathways, such as the mitogen-activated protein kinase cascades, to influence spliceosome activity and modulate transcript isoform ratios. However, the precise components and mechanisms remain undetermined. Together, our work links surface signaling to NLR activation and may be exploited for engineering splicing-regulated immune receptors to enhance disease resistance in crops.

REFERENCES AND NOTES

1. J. D. G. Jones, B. J. Staskawicz, J. L. Dangl, *Cell* **187**, 2095–2116 (2024).
2. J. M. Zhou, Y. Zhang, *Cell* **181**, 978–989 (2020).
3. J. Du *et al.*, *Nat. Plants* **1**, 15034 (2015).
4. S. Kamoun *et al.*, *Mol. Plant-Microbe Interact.* **10**, 13–20 (1997).
5. G. Felix, J. D. Duran, S. Volko, T. Boller, *Plant J.* **18**, 265–276 (1999).
6. Y. Sun *et al.*, *Science* **342**, 624–628 (2013).
7. Z. Chen *et al.*, *Plant Cell* **35**, 1186–1201 (2023).
8. A. Miya *et al.*, *Proc. Natl. Acad. Sci. U.S.A.* **104**, 19613–19618 (2007).
9. T. W. Liebrand, H. A. van den Burg, M. H. Joosten, *Trends Plant Sci.* **19**, 123–132 (2014).
10. M. Yuan, B. P. M. Ngou, P. Ding, X. F. Xin, *Curr. Opin. Plant Biol.* **62**, 102030 (2021).
11. I. M. L. Saur, R. Panstruga, P. Schulze-Lefert, *Nat. Rev. Immunol.* **21**, 305–318 (2021).
12. F. Locci, J. E. Parker, *Open Biol.* **14**, 230387 (2024).
13. M. Yuan *et al.*, *Nature* **592**, 105–109 (2021).
14. B. P. M. Ngou, H. K. Ahn, P. Ding, J. D. G. Jones, *Nature* **592**, 110–115 (2021).
15. H. Tian *et al.*, *Nature* **598**, 500–503 (2021).
16. R. N. Pruitt *et al.*, *Nature* **598**, 495–499 (2021).
17. H. Adachi *et al.*, *eLife* **8**, e49956 (2019).
18. J. Wang *et al.*, *Science* **364**, eaav5868 (2019).
19. J. Wang *et al.*, *Science* **364**, eaav5870 (2019).
20. G. Bi *et al.*, *Cell* **184**, 3528–3541.e12 (2021).
21. H. Böhm *et al.*, *PLOS Pathog.* **10**, e1004491 (2014).
22. I. Albert *et al.*, *Nat. Plants* **1**, 15140 (2015).
23. Y. Sun *et al.*, *Nature* **610**, 335–342 (2022).
24. A. Schultink, T. Qi, A. Lee, A. D. Steinbrenner, B. Staskawicz, *Plant J.* **92**, 787–795 (2017).
25. D. Tang *et al.*, *Nature* **606**, 535–541 (2022).
26. R. Bai *et al.*, *Science* **371**, eabg0879 (2021).
27. R. Bai *et al.*, *Science* **383**, 1245–1252 (2024).
28. P. S. Van Weymers *et al.*, *Front. Plant Sci.* **7**, 672 (2016).
29. J. Ke *et al.*, *Plant Cell* **35**, 2552–2569 (2023).
30. M. Bjornson, P. Pimprikar, T. Nurnberger, C. Zipfel, *Nat. Plants* **7**, 579–586 (2021).
31. F. Liu *et al.*, *Cell* **187**, 4877–4889.e15 (2024).
32. Y. Zhang *et al.*, *Nature* **615**, 884–891 (2023).
33. M. Pais *et al.*, *BMC Evol. Biol.* **18**, 93 (2018).
34. H. Wang *et al.*, *Plant Cell Rep.* **38**, 173–182 (2019).
35. D. Lapin *et al.*, *Plant Cell* **31**, 2430–2455 (2019).
36. J. Wang *et al.*, *Nature* **645**, 737–745 (2025).
37. J. Huang *et al.*, *Mol. Plant* **13**, 1470–1484 (2020).
38. X. Zhong *et al.*, *Nature* **616**, 598–605 (2023).
39. J. Bazin *et al.*, *PLOS Pathog.* **16**, e1008401 (2020).
40. S. I. Kim *et al.*, *Genome Biol.* **26**, 65 (2025).
41. C. Gao *et al*., Surface immune signalling unlocks NLR activation through mRNA alternative splicing, *Zenodo* (2026). https://zenodo.org/records/19688609

ACKNOWLEDGMENTS

We thank S. Kamoun and J. D. G. Jones (The Sainsbury Laboratory), X.-F. Xin (Chinese Academy of Sciences), P. He (University of Michigan), T. Nürnberger (University of Tübingen), and L. Kong (Nanjing Agricultural University) for helpful discussions; Y. Wang (Nanjing Agricultural University), J. H. Vossen, and V. G. A. A. Vleeshouwers (Wageningen University), T. Qi (Tsinghua University), and Z. Tian (Huazhong Agricultural University) for providing plant mutants and materials; Z. Zhang and K. Duan (Nanjing Agricultural University) for providing constructs; and C. He and H. Shu (Nanjing Agricultural University) for bioinformatics suggestions. Data analysis was supported by the Bioinformatics Center of Nanjing Agricultural University. **Funding:** This work was funded by the following: Fundamental and Interdisciplinary Disciplines Breakthrough Plan of the Ministry of Education of China JYB2025XDXM703 (S.D. and Y.W.); National Natural Science Foundation of China 32488302 and 32130088 (S.D.); Joint Research Program of State Key Laboratory of Agricultural and Forestry Biosecurity no. SKLJRP2506 (S.D.); Biotechnology and Biological Sciences Research Council BB/X016382/1 (E.L.H.Y., T.O.B.); National Natural Science Foundation of China 32102234 (C.G.); National Postdoctoral Program for Innovative Talents BX2021131 (C.G.); Agriculture Research System of China CARS-09-P20 (S.D.); Bezos Earth Fund through the Bezos Centre for Sustainable Protein BCSP/IC/001 (T.I.). **Author contributions:** Conceptualization: S.D., T.O.B., C.G.; Methodology: C.G., X.M., X.C., K.L., L.W., E.L.H.Y., N.E., B.S., A.T.; Investigation: S.D., C.G., X.M., X.C.; Visualization: C.G., X.M., X.C., L.W., E.L.H.Y., N.E., A.T., T.I., F.K.; Funding acquisition: S.D., Y.W., C.G., E.L.H.Y., T.O.B., T.I.; Project administration: S.D., T.O.B., C.G.; Supervision: S.D., T.O.B.; Writing – original draft: C.G., T.O.B., S.D.; Writing – review & editing: S.D., T.O.B., L.Y., Y.W., C.G., E.L.H.Y., A.T., N.E. **Competing interests:** T.O.B. is a co-founder of Resurrect Bio Ltd., a company working on NLR biology and crop disease resistance. T.O.B. receives industry research funding unrelated to this study. S.D. is an inventor on patent (ZL 2023 1 1498625.0) held by Nanjing Agricultural University Sanya Research Institute on NLR mRNA splicing. The remaining authors declare no competing interests. **Data, code, and materials availability:** All materials generated in this study are available from the corresponding author upon reasonable request. All data are available in the main text or the supplementary materials. Code can be found at Zenodo (*41*).

SUPPLEMENTARY MATERIALS

science.org/doi/10.1126/science.adx9929
Materials and Methods; Figs. S1 to S19; References (*42*–*60*); MDAR Reproducibility Checklist; Data S1 to S9

Submitted 8 April 2025; resubmitted 19 February 2026; accepted 18 May 2026
10.1126/science.adx9929

Surface immune signaling unlocks NLR activation through mRNA alternative splicing

Chuyun Gao, Xi Meng, Xianchu Chen, Leiyun Yang, Tarhan Ibrahim, AmirAli Toghani, Enoch Lok Him Yuen, Nick Eilmann, Freddie King, Kangping Li, Luyao Wang, Biying Sun, Yuanchao Wang, Tolga Osman Bozkurt, and Suomeng Dong

Science **393** (6806), . DOI: 10.1126/science.adx9929

Editor's summary

Plants use cell surface receptors to detect conserved microbial features and intracellular immune receptors to identify pathogen proteins secreted into the host. Gao *et al*. found that the potato intracellular immune receptor gene *Rpi-vnt1.1* is expressed as two isoforms: one retaining an N-terminal intron and the other with the intron spliced out. The intron-retaining isoform encodes an N-terminal prodomain that prevents oligomerization and autoactivation of the encoded protein. Upon pathogen detection, cell surface signaling promotes intron splicing, removing the prodomain and priming the protein for oligomerization and downstream signaling. The work provides insight into how cell surface signaling regulates intracellular immune receptors in plants, with potential applications for disease-resistance engineering. —Unnati Sonawala and Madeleine Seale

Science (ISSN 1095-9203) is published by the American Association for the Advancement of Science. 1200 New York Avenue NW, Washington, DC 20005. The title *Science* is a registered trademark of AAAS.